Accepted Manuscript

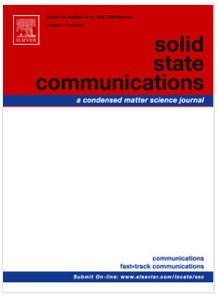

Compositional patterning in coherent and dislocated alloy nanocrystals

N.V. Medhekar, V. Hegadekatte, V.B. Shenoy

PII: S0038-1098(09)00257-9
DOI: 10.1016/j.ssc.2009.04.044
Reference: SSC 10092

To appear in: *Solid State Communications*

Received date: 3 April 2009
Accepted date: 27 April 2009

Please cite this article as: N.V. Medhekar, V. Hegadekatte, V.B. Shenoy, Compositional patterning in coherent and dislocated alloy nanocrystals, *Solid State Communications* (2009), doi:10.1016/j.ssc.2009.04.044

Compositional patterning in coherent and dislocated alloy nanocrystals

N. V. Medhekar[a], V. Hegadekatte[a], V. B. Shenoy[*,a]

[a]*Division of Engineering, Brown University, Providence, RI-02912.*

Abstract

Variations in the distribution of the alloy components can significantly influence the electronic properties of the self-organized alloy nanocrystals. Using a combination of finite element and quadratic programming optimization methods, we have developed an efficient numerical technique to compute the equilibrium composition profiles in coherent and dislocated nanocrystals. We show that the variations in composition profiles arise due to the competition between chemical mixing effects and the relaxation of composition-dependent mismatch strain as well as strain due to dislocations. We find that the composition profiles in these crystals depend strongly on the morphological features such as the slopes and curvatures of their surfaces and the presence of corners, edges and dislocations at the nanocrystal–substrate interface. This approach provides a means for the quantitative description of the factors controlling equilibrium composition profiles in various coherent and dislocated self-organized alloy systems.

1. Introduction

A particularly appealing approach to manufacturing nanoscale devices is to exploit the natural tendency of small material clusters to self-organize. While it is well-known that strain-driven self assembly can give rise to nanoscale pattern formation of 2D domains and pattenrs [1], it also provides a versatile means to fabricate nanoscale islands in lattice-mismatched semiconductor *alloy* systems which can serve as functional elements in optical, electronic and photo-voltaic devices [2, 3]. The electronic structure of these nanoscale islands or nanocrystals is strongly influenced by the shape, elastic deformation and most importantly by their composition, thereby enabling the device properties to be controlled. A tighter control of these characteristics significantly reduces power consumption and heat generation, while the small dimensions of the devices allow order of magnitude advances in miniaturization. Self assembled SiGe [4, 5, 6] and InGaAs [7] quantum dots have received particular attention as the former material system can be readily integrated with the well developed Si integrated circuit technology while the latter has been successfully applied in photovoltaic and photonic bandgap applications.

The past few years have seen tremendous advances in development of processing and patterning techniques that lead to a uniform array of nanocrystals of nearly identical shapes and sizes [40, 8]. However, key factors that play a role in controlling the variations in composition within the nanocrystals remain poorly understood. A quantitative determination of the composition profiles is critical in device applications as variations in composition at the nanoscale can substantially influence the electronic properties (for example, excitonic transitions [9], electron-hole band alignment and band gaps [10]) and therefore directly influence the performance of devices. While there is a large body of theoretical work on the formation and growth of nanocrystals, almost all of it neglects alloying effects by assuming a uniform composition distribution within the crystals.

In recent years, considerable progress has been made in measuring the composition profiles within individual quantum dot nanocrystals with nanoscale resolution [11, 12, 13, 14, 15, 16, 17]. These experimental studies show two distinct types of scenarios. The work of Stanley Williams and coworkers using x-ray scattering and independent selective etching techniques [12, 15, 17] shows a Si-rich core covered by a Ge-rich shell for dome shaped SiGe quantum dots at 600 °C. In distinct contrast, the work of Schmidt and coworkers using a combination of selective wet chemical etching and atomic force microscopy [13, 14] shows that for pyramid and dome shaped islands, the corners are highly intermixed, whereas the edges, apex and the center of the pyramids remain Ge rich at 550 °C. Given the sensitivity of the composition profiles in the nanocrystals to growth conditions and the differences between the experimental measurements from different groups, information from these experiments can only be properly interpreted with models that can distinguish the differences between composition profiles under different growth conditions. To that end, a key question that one is generally faced with in these experiments is whether or not a measured profile is close to equilibrium.

As alloy nanocrystals continue to grow, dislocations can nucleate to relax the elastic strain energy in the crystal and the substrate [18]. It is known that depending on the average composition in the nanocrystal and its size, there can be one or more loops of dislocations at the interface with the substrate [19, 20]. Such tree-ring interface dislocation structures and the critical crystal size for their nucleation [21] have been well studied for SiGe quantum dots. Since dislocations give rise to their own characteristic strain fields, the nucleation of a dislocation during growth can signicantly alter the strain and therefore the composition distribution in an alloy nanocrystal. Most of the

Email addresses: vivek_shenoy@brown.edu (V. B. Shenoy)

work concerning dislocations in alloy nanocrystals typically assumes a uniform composition throughout the crystal; experimental studies measuring the composition profiles in individual dislocated nanocrystals have been far fewer compared to the coherent crystals. For example, it has recently been shown that for both coherent and dislocated SiGe nanocrystals, the Ge mole-fraction decreases while moving from apex towards the substrate; however, coherent crystals are characterized by a sub-linear variation, while dislocated crystals show a plateau in the composition in near-apex region [22]. In order to understand such nanoscale variations in composition in dislocated crystals and the factors controlling them, one needs to carefully analyze the coupling between the elastic fields due to the dislocations and due to the composition variations in equilibrium.

In equilibrium, for a given size and shape of the crystal, the composition profile is obtained by minimizing the total free energy that consists of the elastic energy and entropic and chemical mixing energies. The primary difficulty in obtaining composition profiles is that the shape, strain and composition are all coupled to each other. Furthermore, in equilibrium, the total free energy has to be minimized by holding the overall ratio of the alloy components in the dot at a fixed level, making the optimization problem even more difficult. In addition, the coupling between the strain fields arising due to dislocations and due composition variations in dislocated nanocrystals adds to complexity of the optimization problem. Subsequently, only calculations that adopt a number of simplifying assumptions are available. For the case of coherent crystals, these approximations include small slopes of the sidewalls of the quantum dots [23] and linear extrapolation of the composition profiles from the surface to the bulk [24]. The approximations made in the calculations allow only for the analysis of pre-pyramid clusters with very shallow side-walls. In the case of dislocated crystals, approximate strain fields obtained by assuming a dislocation lies at the center of solids with simple shapes such as a cylinder, have been employed to compute their contribution to the total elastic energy of the system. Monte Carlo methods have also been employed to analyze quasi-equilibrium composition profiles [25, 26], but the long range nature of the elastic interactions makes statistical sampling of the large configuration space (required to obtain properly averaged composition maps in realistic structures) a very demanding and tedious task.

Here we study equilibrium composition maps in alloy nanocrystals by employing the finite element method for rigorous treatment of elastic fields without any restrictions on their shape and an optimization scheme based on quadratic programming methods. A brief account of the key results for composition maps in coherent alloy quantum dots is described in our earlier work [27]. We find that the shapes of the crystals play a very important role in determining the degree of alloy decomposition that can be achieved at a given temperature. The composition profiles in faceted quantum dot crysytals with steep side-walls are found to be characteristically different from the corresponding case of shallow dots. In the former case, segregation of the larger alloy component in the tensile regions of the quantum dot leads to the formation of 'cusped' composition profiles which manifest in the form of dimpled surface profiles upon selective etching of one of the alloy components (Fig. 1). Shallower crystals on the other hand, are less decomposed and yield surface profiles with large etch pits. Both of these features have been observed during wet chemical etching of SiGe quantum dots [12, 13, 15].

In order to guide the interpretation of composition maps measured in experiments, the degree of alloy decomposition in faceted nanocrystals is presented in a phase diagram plotted in the space spanned by the orientation of their side-walls and temperature. Based on this phase diagram, the effect of decomposition on the shape transition between quantum dots with different facet orientations is computed—alloy decomposition is found to significantly decrease the transition volumes for shape transformation. To further demonstrate the role of shape and strain on alloy decomposition at the nanoscale, we have considered the composition profiles of dome, truncated pyramid and unfaceted pre-pyramid or Gaussian shaped quantum dots nanocrystals, all of which have been observed in SiGe [4, 5, 28, 29] and InGaAs [29, 30] systems. In the case of dome and truncated-pyramid shaped quantum dots with multiple facets, we find a rich array of compositional patterns with enrichment of the larger alloy component at the corners and edges formed by the intersection of different facets. In the case of unfaceted quantum dots, both the slopes and curvatures of the surface are found to influence compositional patterning. Finally, composition maps in dislocated nanocrystals are significantly different that maps in coherent crystals and are found to strongly depend on number of dislocations and the growth temperature.

This paper is organized as follows. In section 2, we present the mathematical formulation and the optimization procedure for computing the equilibrium composition profiles in ally nanocrystals. Section 3 is devoted to the composition maps in coherent nanocrystals, while composition maps in dislocated nanocrystals are briefly illustrated in section 4. In section 5, we summarize the key results of our work.

2. Mathematical formulation for equilibrium composition profiles in alloy nanocrystals

For an AB alloy nanocrystal grown epitaxially on a substrate of species A, the total free energy E of the quantum dot-substrate system can be written as $E = E_{ch} + E_{el} + E_s$, where E_{ch} is the chemical free energy of the alloy components in the nanocrystals, E_{el} is the elastic strain energy due to the lattice mismatch between the quantum dot and the substrate, and E_s is the surface energy cost involved in the formation of the nanocrystal. In the epitaxially mismatched alloy systems, elastic fields tend to favor segregation of the alloy component with larger (smaller) lattice constant near more tensile (compressive) regions in the crystal. On the other hand, the thermodynamic mixing free energy (which depends on temperature) can prevent the decomposition of the alloy. In equilibrium, for a given shape of the crystal, the composition profiles are determined by the competition between these two contributions.

In general, the functional form of the thermodynamic mixing free energy of the alloy, which includes both enthalpic and en-

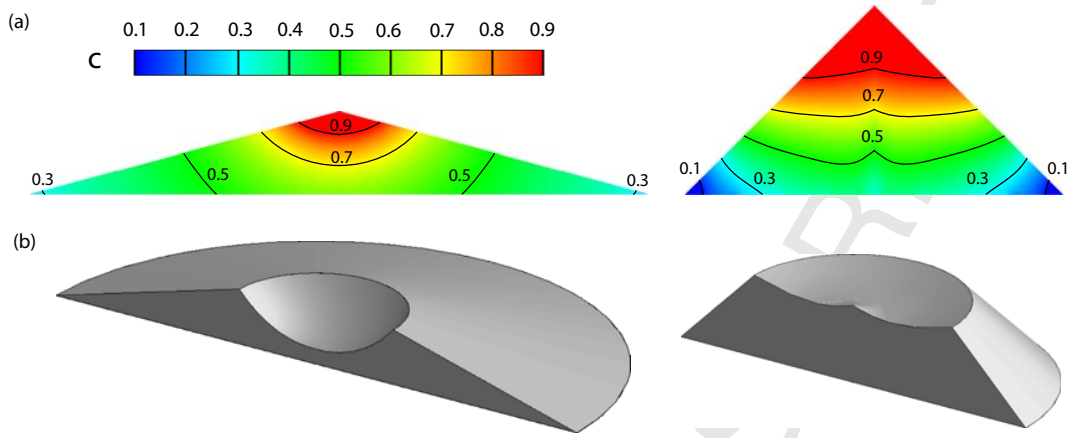

Figure 1: Influence of morphology on the equilibrium composition profiles in alloy nanocrystals [27]. (a) Composition profiles in axially symmetric quantum dots of identical size, but with shallow (left) and steep side-walls (right). The steeper side-walls allow for larger strain relaxation resulting in a greater degree of segregation of alloy components at the apex and in the periphery of the nanocrystal. The composition profiles are obtained for $F_0 = -0.2$ and with average composition $\bar{c} = 0.5$. (b) The 3D rendering of the shapes of the quantum dots in (a) upon etching with a selective chemical agent that dissolves regions of dot whose composition, c, exceeds 65%. The segregation indices (Eq. 4) for the steep and shallow dots are 0.177 and 0.051, respectively.

tropic contributions, can be quite involved, although the latter contribution dominates at high temperatures, favoring complete mixing of the alloy components. In order to capture the key aspects of mixing effects, we write the chemical free energy of the alloy nanocrystal as in our earlier work as

$$E_{ch} = \int_{V_c} f(c)\, dV, \tag{1}$$

where V_c is the volume of the crystal, $c(\mathbf{x})$ is the mole fraction (or composition) of the B-species in the alloy and the free energy density is taken to be $f(c) = \Delta F(T)\, c + F_m(T)\, c(1-c)$. Here, $\Delta F(T)$ is the free energy difference between the phases A and B while the temperature (T) dependent parameter $F_m(T)$ determines stability of the alloy to phase separation. That is, for $F_m > 0$ the alloy thermodynamics favors phase separation into A and B components, while $F_m < 0$ results in complete mixing of alloy components at any composition. For typical semiconductor alloy systems such as SiGe and InGaAs, the coefficient $F_m(T)$ is obtained by fitting $f(c)$ to the mixing energy density, $\Omega c(1-c)+(k_BT/v_a)\left[c\log c + (1-c)\log(1-c)\right]$, where the regular solution interaction parameter Ω is taken to be [23] 3.47 and 4.12 $\times 10^8$ Joules/m^3 for SiGe/Si and InGaAs/GaAs, respectively and v_a is the atomic volume. Note that the contribution to the total energy of the nanocrystal from the first term in $f(c)$ is $\Delta F(T)\bar{c}V_c$, where $\bar{c}$ is the average composition in the crystal. If the average composition is specified, this term is independent of the composition profile in the crystal and therefore does not play a role in the determination of the equilibrium distribution of alloy components. In the subsequent sections, we will consider the composition profiles for both positive and negative values of F_m, representative of the thermodynamics of mixing at low and high temperatures, respectively.

In a nanocrystal strained due to the epitaxial mismatch with the substrate, the regions near its sidewalls are in a relatively relaxed state of strain compared to the core regions. While the relaxation of mismatch strain substantially lowers elastic energy in the nanostructure, it also results in a strained substrate due to the coherent nature of the nanocrystal–substrate interface. Furthermore, the dislocations at the interface also cause additional elastic strain fields in the nanocrystal as well as the substrate. Therefore, the elastic energy of the composite nanocrystal-substrate system can be written as

$$E_{el} = \frac{1}{2}\int_{V_c+V_s} C_{ijkl}(\epsilon^0_{ij} + \epsilon^r_{ij})(\epsilon^0_{kl} + \epsilon^r_{kl})\, dV\,, \tag{2}$$

where ϵ^0_{ij} is the strain in the absence of relaxation due to sidewalls or free surfaces, while ϵ^r_{ij} is the relaxation strain. ϵ^0_{ij} has the contributions from composition-dependent mismatch strain and the strain fields due to dislocations, and can be written as $\epsilon^0_{ij} = \epsilon_m c(\mathbf{x})\delta_{ij} + \epsilon^d_{ij}$. Here ϵ_m is the equi-biaxial mismatch strain arising due to the difference in the lattice constants of the two species, and ϵ^d_{ij} is the strain field due to dislocations in an isotropic linear elastic full space. In our calculations, the island and the substrate are assumed to be isotropic linear elastic materials with an identical elasticity tensor C_{ijkl}.

While it is relatively straightforward to compute the strain in the absence of any relaxation due to sidewalls or free surfaces of the nanocrystal (i.e. ϵ^0_{ij}), computing relaxation strain ϵ^r_{ij} is quite complicated due to the strong coupling between the relaxation and the shape of the nanocrystal. We have therefore numerically obtained the elastic fields using finite element methods (Fig. 2) by treating the composition-dependent mismatch strain and the strain due to dislocations as the initial strain in an infinitely large solid. At the same time, traction-free boundary conditions are imposed on the free surfaces of the nanocrystal and the substrate. The relaxation strain ϵ^r_{ij}, thus computed, ac-

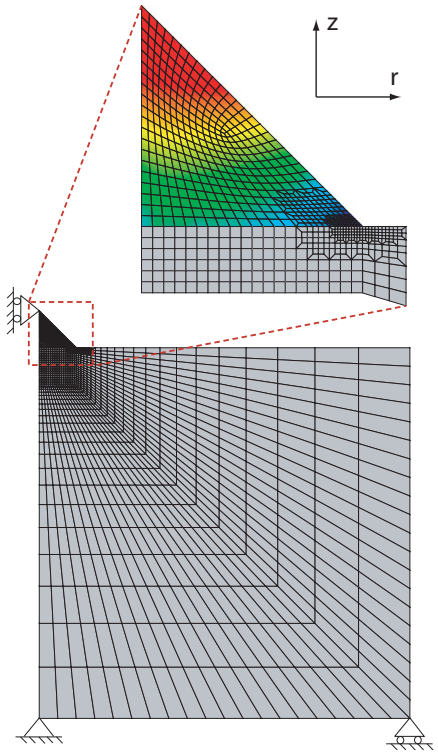

Figure 2: The finite element mesh used for the computation of the elastic fields for a coherent, axially symmetric quantum dot crystal. The volume of the substrate used in the calculations is three orders of magnitude larger than the volume of the quantum dot, so that finite-size effects are negligible.

counts for both the correction to the field of dislocation in an infinite solid and the strain relaxation due to shape as well as from variations in composition. For accurate computation of elastic fields, a non-uniform meshing scheme is employed with greater mesh density in the regions of high stress concentration such as the peripheral regions of the nanocrystal near the base (Fig. 2) and the dislocation cores.

For a given shape and size of the nanocrystal, the equilibrium composition profiles are determined by minimizing the sum of the chemical (Eq. 1) and elastic (Eq. 2) energies with respect to local composition $c(\mathbf{x})$ while constraining the average composition within the nanocrystal. For this non-linear constrained optimization problem, we use a sequential quadratic programming method [31]. The gradients of the energy function and the constraints required for the optimization method are computed numerically. This numerical optimization method is quite robust and along with accurate computation of elastic fields using finite element methods, it allows us to determine the equilibrium composition profiles for any shape. With this method, the approximations in computing the elastic fields such as assuming small slopes of the nanocrystal sidewalls [23] or using the elastic fields of a dislocation at the center of a cylinder [21], are therefore not necessary. Next, we describe in detail the composition maps in coherent nanocrystals with various shapes observed in experiments.

3. Composition maps in coherent nanocrystals

3.1. Influence of nanocrystal morphology on composition maps

The role of shape on the distribution of the alloy components is first considered for the case of cone-shaped coherentquantum dot nanocrystals shown in Fig. 1. The composition profiles in these dots depend only on three parameters, namely, the average composition $\bar{c}$, the sidewall angle θ and the ratio of the chemical and elastic energy densities, $F_0 = F_m/(M\epsilon_m^2)$, where M is the biaxial modulus. This observation follows from the fact that the chemical and the elastic energies (Eqs. 1 and 2) scale linearly with the volume of the coherent nanocrystal which allows us to write their sum in the form

$$E_{ch} + E_{el} = M\epsilon_m^2 V_c \; \hat{W}(\bar{c}, \theta, F_0), \tag{3}$$

where $\hat{W}$ is a dimensionless function. Since this function does not depend on size, the equilibrium composition profile in a "faceted" quantum dot with a given sidewall angle θ is independent of its volume, V_c.

The equilibrium composition profiles in 50-50 alloy quantum dots with sidewall angles of 15°and 45°are shown in Fig. 1(a). Here, we have taken $F_m = -0.2\, M\epsilon_m^2$, so that alloy thermodynamics favors complete mixing. However, strain leads to segregation of the larger alloy component (B) at the apex while the corners of the dot near the substrate are enriched in the other component (A). The degree of decomposition depends on the shape—segregation of the alloy components at the apex and at the periphery is much larger in the steeper dot. The 50% isocomposition profile in this case is located nearly half way between the substrate and the apex of the dot, while this profile in the shallower case lies between the axis of symmetry and the periphery of the dot. Furthermore, the isocomposition profiles that lie above the substrate in the steeper dot develop a "cusp" at the axis of symmetry. This feature, which is absent in the shallower dot, should be observed by etching the structures with a selective chemical agent that removes material above a threshold level of composition. The 65% isocomposition surface profiles given in Fig. 1(b) for the two cases show very distinct shapes—the steeper dot develops a nearly flat top with a 'dimple' along its symmetry axis, whereas a deep pit is formed in the shallower dot. Similar features of etched surfaces have been observed in dome and pyramid shapes SiGe quantum dots, respectively [12, 13, 15, 16]. However, kinetic effects, for example the smaller diffusion length of Ge compared to Si can also possibly give similar shapes upon selective etching [16]. Further experiments that consider the surface profiles as a function of annealing time are needed to determine if the measurements correspond to equilibrium predictions.

3.2. Compositional phase diagrams

Strain-induced alloy segregation in coherent nanocrystals can be analyzed in a quantitative manner by considering the

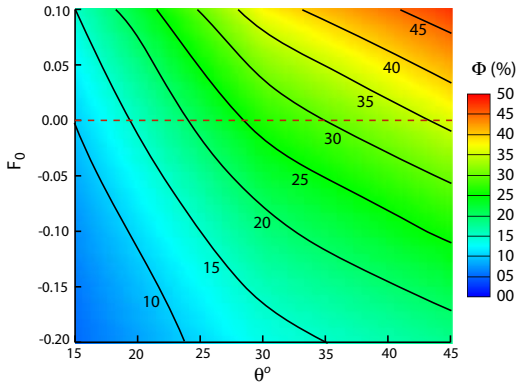

Figure 3: Compositional phase diagram showing degree of segregation, Φ as a function of the parameter F_0 and the shape of the quantum dot crystal represented by the angle of side-walls, θ. Even when the thermodynamic mixing energy favors mixing ($F_0 < 0$), the relaxation of strain for quantum dots with steep side-walls results in the alloy segregation within the quantum dot. Similarly, when thermodynamics favors phase separation ($F_0 > 0$), complete decomposition is not observed. The average composition of the quantum dot $\overline{c}$ is 0.5.

segregation index Φ, which we define as

$$\Phi(F_0, \theta) = \frac{4}{V_c} \int_{V_c} (c(\mathbf{x}) - \overline{c})^2 \, dV \,. \tag{4}$$

For a 50-50 alloy nanocrystal, the alloy components are completely mixed (i.e. $c(\mathbf{x}) = 0.5$ everywhere) when $\Phi = 0$, while $\Phi = 1$ corresponds to complete alloy decomposition. The computed level curves of the segregation index are plotted in Fig. 2 as a function of the ratio F_0 and the facet angle, θ and segregation indices for InGaS and SiGe quantum dots at typical growth temperatures are given in Table 1. As anticipated, the segregation index increases with increasing θ, but complete segregation of the alloy components is not achieved even when alloy thermodynamics favors phase separation ($F_0 > 0$). Similarly, complete mixing is only seen for very shallow structures when F_0 is sufficiently negative.

To understand why complete segregation is not observed when thermodynamics favors alloy decomposition ($F_0 > 0$), we consider the elastic energy of a nominally flat 50-50 alloy film in two extreme cases: a) when the composition in the film is uniform and b) the film is completely phase separated (refer to Fig. 3). In the former case, the elastic energy per unit volume of the film is $M\epsilon_m^2/4$, while in the latter case it is $M\epsilon_m^2/2$. Clearly, because of the quadratic scaling of the strain energy density with the composition dependent mismatch strain, $c\epsilon_m$, a completely mixed alloy film has lower elastic energy than a phase separated film. Therefore, in the absence of in-plane strain relaxation, the elastic contribution to the total free energy always favors uniform composition even when alloy thermodynamics favors decomposition. Phase separation cannot occur unless the energetic gain from thermodynamics is sufficiently large, or when the condition $F_m > M\epsilon_m^2$ is satisfied. Extending this argument to the case of nanocrystals whose shapes allow for strain relaxation, one can see that complete phase separation can only be achieved when the parameter, F_0 is sufficiently large. Next, we show that strain-induced segregation in quantum dot crystals can substantially reduce the critical size for transition between the shapes with different facets.

	InGaAs/GaAs			SiGe/Si		
T	$M\epsilon_m^2$	F_m	$\Phi(30°)$	$M\epsilon_m^2$	F_m	$\Phi(30°)$
400 °C	4.86	-0.80	0.151	2.82	-3.00	0.021
600 °C	4.86	-1.91	0.075	2.82	-4.90	0.010

Table 1: Segregation index for InGaAs/GaAs and SiGe/Si quantum dots with sidewall angles of 30°. The strain energy density, $M\epsilon_m^2$ and the coefficient of the mixing energy,[**?**] F_m are in given units of 10^8Joules/m^3. The table shows that the degree of decomposition is considerably greater in InGaAs nanocrystals compared to SiGe crystals at typical growth temperatures.

3.3. Role of composition maps in shape transitions in nanocrystals

It is well known that with increasing size, shallow SiGe and InGaAs quantum dot crystals transform to steeper domes [4, 5, 28, 29, 30], as strain can be more efficiently relaxed in the latter case. The critical volume for shape transition depends on the surface energies of the facets and the nominally flat film, which, in general, can all be different from each other. However, the key features of this transition can be studied by assuming that all the surface energies involved are equal [32]. In this case, for dots with uniform composition, shape transitions occur at a size when the gain in the elastic energy obtained by the formation of the steeper dots offsets the cost of forming the sidewall surfaces. However, if the decomposition of the alloy is permitted, one can see that steeper dots allow for even larger reduction of the elastic energy as the alloy components can redistribute themselves more readily to strain-relaxed regions (Fig. 1). Using the dimensionless function $\hat{W}$ (Eq. 3) obtained from our optimization procedure, the total energy of an alloy dot can then be expressed as

$$E = M\epsilon_m^2 V_c \; \hat{W}(\overline{c}, \theta, F_0) + \gamma \, V_c^{2/3} \hat{\Gamma}(\theta) \,, \tag{5}$$

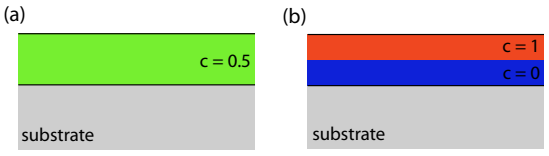

Figure 4: Schematic of an epitaxial lattice mismatched film of uniform thickness with (a) uniform composition ($c = 0.5$) and (b) complete alloy decomposition into individual components. Elastic energy is lower for the former configuration due to quadratic scaling of the strain energy density with the composition dependent mismatch strain, $c\epsilon_m$.

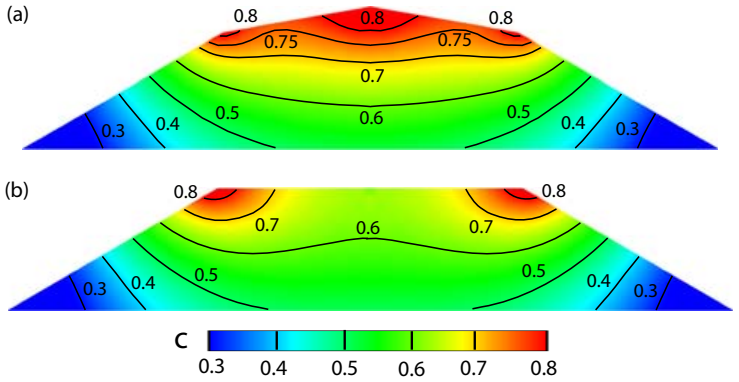

Figure 6: Equilibrium composition profiles in axisymmetric quantum dot crystals with (a) "dome" shape, the angles of the side-walls being 30^o and 15^o, and (b) a truncated-cone shape with a sidewall angle of 30^o. While the composition profiles are similar near the base, larger strain relaxation in the regions near the corners results in a greater segregation in the apex of the dome-shaped crystals. The composition profiles are obtained for $F_0 = -0.2$ and the average composition is $\bar{c} = 0.5$.

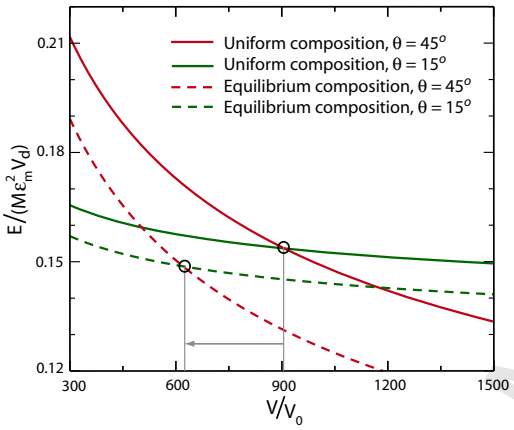

Figure 5: Variation of the energy per unit volume for quantum dot crystals with shallow and steep side-walls ($\theta = 15°$and $\theta = 45°$, respectively) as a function of their size (normalized by the characteristic volume, $V_0 = [\gamma/(M\epsilon_m^2)]^3$. The total energy of the decomposed dots (dotted lines) is lower than the energy of dots with uniform composition, $\bar{c} = 0.5$ (bold lines). However, the reduction in the energy is greater for the steeper dot, resulting in smaller critical size for transition in shape. The surface energies for shallow and steep side-walls are assumed to be identical and the mixing parameter $F_0 = -0.2$.

where the surface energy, γ, is assumed to be independent of the facet angle, θ and

$$\hat{\Gamma}(\theta) = \pi\left(\frac{3}{\pi\tan(\theta)}\right)^{2/3}\left(\sqrt{1+\tan^2(\theta)} - 1\right). \qquad (6)$$

A plot of the energy per unit volume of decomposed dots in Fig. 4 (for $F_0 = -0.2$) shows that the volume to transition from a sidewall angle of 15° to 45° reduces by nearly 30% relative to the transformation volume of the to the dots with uniform composition.

3.4. Composition maps in faceted and Gaussian-shaped nanocrystals

In equilibrium, SiGe and InGaAs nanocrystals can also adopt shapes that consists of two or more facet orientations [4, 5, 28, 29, 30]. The computed equilibrium composition maps in such dome and truncated-pyramid shaped quantum dot crystals are shown in Fig. 5. A distinguishing feature of these dots is the intricate pattern of isocomposition profiles that can be attributed to the presence of "corners" formed by the intersection of different facets. Since such corners allow for relaxation of mismatch strain, the free energy can be lowered by segregation of the larger alloy component in these regions. The number of extrema in the composition maps can therefore be directly correlated to the occurrences of facet intersections in the dot shape. The composition profiles in the regions close to the periphery of the base, however, are similar to the corresponding profiles in cone-shaped quantum dot in Fig. 1.

Finally, we consider the equilibrium composition profiles in Gaussian "pre-pyramid" quantum dots whose mean curvature varies in a non-monotonous manner from the apex to the base. Such shapes are typically observed in early stages of growth of the nanocrystals [6]. The composition maps in two such dots of identical size but with different aspect ratios (the ratio of the height to the base width) are shown in Fig. 7. In both cases, a local extremum in composition is seen close the point of inflection as a result of the competition between elastic and capillary effects—the former favors segregation of the B atoms in convex regions, while the latter tends to move these atoms to concave regions. A balance of these effects close to the points of inflection leads to the observed equilibrium profiles with extrema at the surface of the dot. As in the case of the faceted islands (Fig. 1), the degree of decomposition is greater in the steeper dot as evidenced by the location of the 50% isocomposition line—for the steeper dot it is located above the substrate, while it is closer to the axis of symmetry in the case of the shallower dot. In this regard, the profiles obtained by computing strain fields by assuming small surface slopes[23] are different even from the profiles for the shallow dot in Fig. 7 whose height to width ratio is only 0.23. While 50% isocomposition line obtained in the small-slope limit is vertical and is located nearly mid-way between the axis of symmetry and the edge of the dot, this line in Fig. 7(a) is curved and is closer to the axis of symmetry, indicating that the composition profiles are very sensitive to the strain fields in the crystals.

The discussion so far was focused on the competition be-

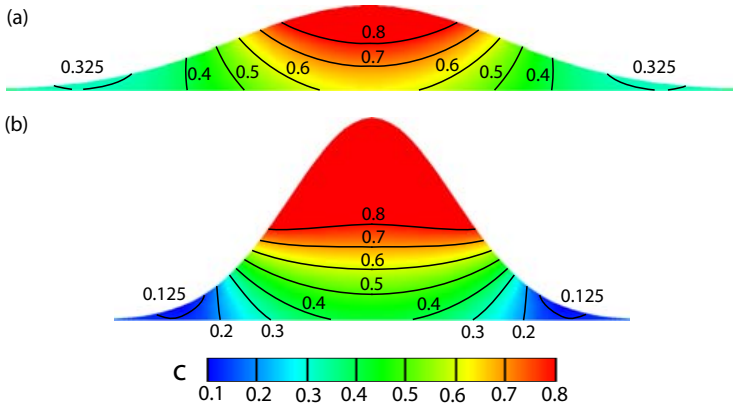

Figure 7: Equilibrium composition profiles in axisymmetric Gaussian pre-pyramid quantum dot nanocrystal (a) with aspect ratio (ratio of the height to width) of 0.12, and (b) with larger aspect ratio of 0.39. In the shape with smaller aspect ratio (part a), the regions near the base are considerably mixed, while the central region forming the core is rich in species B. Due to greater strain relaxation in the shape with larger aspect ratio (part b), species B segregates largely near the apex leaving the core regions near the base rich in species A. The composition profiles are obtained for $F_0 = -0.2$ and the average composition is $\overline{c} = 0.5$.

tween the thermodynamic mixing and the strain relaxation in coherent alloy nanocrystals in controlling the composition variations in nanocrystals. However, as nanocrystals grow to a large size, nucleation of dislocations at the nanocrystal–substrate interface can provide a mechanism to lower the increased strain energy. Next, we briefly describe how the interplay between the elastic fields of interface dislocations and the alloy thermodynamics can influence the composition maps in alloy nanocrystals.

4. Composition maps in dislocated nanocrystals

First we consider a nanocrystal with interface dislocations as a model system to understand the composition distribution in large SiGe and InGaAs quantum dots. These nanocrystals have been observed to have a tree-ring dislocation structure at the nanocrystal–substrate interface [19, 20]. While dislocated nanocrystals usually have dome or truncated dome like shapes, our earlier analysis (Figs. 1 and 6) shows that the composition profiles in the dome-shaped quantum dots are qualitatively similar to the profiles in the conical dots except in the near-corner regions. We therefore consider a simple case of triangular-shaped quantum dot with two interface edge dislocations in plane strain condition [33] as shown in Fig. 8. The size of the quantum dot is chosen to be such that the formation of dislocations is indeed energetically favorable.

As in the previous cases of composition maps in coherent nanocrystals, first we focus on the case where $F_m = -0.2\, M\varepsilon_m^2$ to compare the competing influences of strain field due to dislocations and due to elastic mismatch. We use the parameters that are typical to the SiGe system, namely, Burger's vector $b = 0.39$ nm and the mismatch strain $\epsilon_m = 0.042$. Fig. 8 shows the distribution of alloy components in a dislocated quantum dot. For a comparison, we have also shown the equilibrium composition profiles in a coherent dot of same size and shape. The composition profiles in the dislocated dot are characterized by a relatively mixed apex region and the strong localization of the larger alloy component near the dislocation core. This can be attributed to the fact that the dislocations reduce the overall strain in the dot which makes the segregation-driving effects of strain relaxation less dominant. However, the strain in small regions near the dislocation core is largely tensile, thereby inducing a localized segregation of the larger alloy component which relaxes the tensile strain. Nevertheless, a small region near the apex of the dot remains richer in one component as confirmed by experiments where enrichment of Ge is observed in $Si_{1-x}Ge_x$ dislocated quantum dots [22].

Next, we consider how the mixing energy parameter F_0 in Eq. (3) influences the composition profiles in dislocated nanocrystals. Fig. 9 presents the composition profiles in a triangular-shaped quantum dot with four interface edge dislocations computed for three different values of the parameter F_0. Fig. 9(a) with $F_0 = -1.06$, which is typical for SiGe system at the growth temperature 400 °C, shows that the components are well-mixed in a large portion of the dot. However, as F_0 increases (or as the temperature decreases), the alloy segregation also increases as evident from the Figs. 9(b) and 9(c). This behavior is essentially consistent to the compositional phase diagram for coherent nanocrystals shown in Fig. 3, except in the fact that the regions near the dislocation cores remain enriched with larger alloy component even at high growth temperatures. As the parameter F_0 increases (or as the growth temperature reduces), the energy gain due to strain relaxation more than offsets the mixing energy cost due to alloy segregation, resulting in a strain-relaxed crystal with segregated composition profiles. This suggests that nanocrystals grown at low temperatures can actually be more relaxed compared to the crystals grown at higher temperatures as observed in dislocated Ge/Si(001) islands [34]. However, slow kinetics of growth—especially at low growth temperatures—can limit the degree of alloy segregation that can be achieved.

A close comparison of Figs. 8(b) and 9(b) also shows the effect of introducing more dislocations on composition profiles. With more dislocations, the strain in the nanocrystal can be effectively relaxed resulting in a relatively uniformly mixed distribution of alloy components. However, dislocations can only be nucleated as a result of increased strain in the nanocrystal as it grows, which in turn can stabilize steeper facets and drive the segregation of alloy components as we have seen earlier. Therefore, in situations where the growth is close to equilibrium,

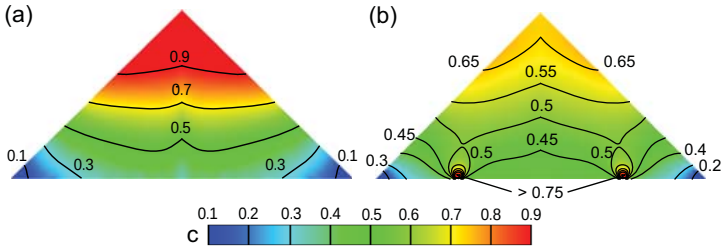

Figure 8: Equilibrium composition profiles in a coherent (a) and dislocated nanocrystal (b) of the same size and shape. The composition profiles are significantly altered in the presence of interface edge dislocations with a considerable mixing of alloy components near the apex and a localized segregation near the dislocation cores. The base width of islands is 50 nm and the side wall angle θ is 45°. The composition profiles are obtained for a misfit strain $\varepsilon_m = 0.042$, $F_0 = -0.2$ and the average composition of $\bar{c} = 0.5$. The dislocations, with Burger's vector $|b| = 0.39$ nm, are located midway from the core of the quantum dot towards its periphery.

along with oscillations in shape [19], the composition profiles can be expected to alternate between relatively uniform profiles after nucleation of a dislocation and the segregated profiles as the nucleation of subsequent dislocation becomes eminent.

5. Summary

To summarize, we have developed an efficient method to compute composition maps in strained alloy quantum dots and nanocrystals. We have shown that the composition profiles depend strongly on the slopes and curvatures of the surfaces of these structures as well as the presence of other geometric features such as corners and edges. In the case of dislocated nanocrystals, the coupling between strain field due to dislocations and due to the composition-dependent mismatch can lead to significant transformation in the composition profiles compared to the coherent nanocrystals. Our approach provides a means to rigorously study the interdependence of the shape, strain, and composition in the lattice mismatched systems and can help interpret the measured composition profiles. The method can therefore be employed to analyze compositional patterning in small scale structures such as nanowires [35], nanorings [36], nanotrees [37], quantum fortresses [38], quantum posts [39], and quantum dot molecules [40].

The next step in the analysis of such structures is to extend our method to include the dynamics of compositional patterns under non-equilibrium growth conditions. If the composition maps obtained using this approach are coupled with electronic structure calculations, a complete *in silico* characterization of the devices from growth to final performance can be achieved.

6. Acknowledgments

The research support of the NSF through the Brown University MRSEC program and the grant CMMI 0855853 is gratefully acknowledged.

References

[1] M. Seul, D. Andelman, Science 267 (1995) 476.
[2] W.D. Heiss, Quantum dots: a door way to nanoscale physics, Springer, 2005.
[3] Z.M. Wang, Self-Assembled Quantum Dots (Lecture Notes in Nanoscale Science and Technology), Springer, 2007.
[4] G. Medeiros-Ribeiro, M. Bratkovski, T.I. Kamins, D.A.A. Ohlberg, R.S.Williams, Science 279 (1998) 353.
[5] F.M. Ross, R.M. Tromp, M.C. Reuter, Science 286 (1999) 1931.
[6] J. Drucker, IEEE J. Quan. Elec. 38 (2002) 975.
[7] J. Stangl, V. Holy, G. Bauer, Rev. Mod. Phys. 76 (2004) 725.
[8] D. Grützmacher, T. Fromherz, C. Dais, J. Stangl,E. Müller,Y. Ekinci, H.H. Solak, H. Sigg, R.T. Lechner, E. Wintersberger, S. Birner, V. Hol, G. Bauer, Nano Lett. 7 (2007), 3150.
[9] J. Shumway, A.J. Williamson, A. Zunger, A. Passaseo, M. Degiorgi, R. Cingolani, M. Catalano, P. Crozier, Phys. Rev. B. 64 (2001) 125302.
[10] W. Sheng, J.-P. Leburton, Phys. Rev. B 63 (2001) 161301.
[11] M. Floyd,Y. Zhang, K.P. Driver, J. Drucker, P.A. Crozier, D.J. Smith, Appl. Phys. Lett. 82 (2003) 1473.
[12] A. Malachias, S. Kycia, G. Medeiros-Ribeiro, R. Magalhães-Paniago, T.I. Kamins, R.S. Williams, Phys. Rev. Lett. 91 (2003) 176101.
[13] U. Denker, M. Stoffel, J. Tersoff, G. Katsaros, G. Costantini, K. Kern, N.Y. Jean-Phillipp, D.E. Jesson, O.G. Schmidt, Phys. Rev. Lett. 94 (2005) 4.
[14] U. Denker, A. Rastelli, M. Stoffel, O.G. Schmidt, Phys. Rev. Lett. 90 (2003) 196102.
[15] M.S. Leite, G. Medeiros-Ribeiro, T.I. Kamins, R.S. Williams, Phys. Rev. Lett. 98 (2007) 165901.
[16] G. Katsaros, G. Costantini, M. Stoffel, R. Esteban, A.M. Bittner, A. Rastelli, U. Denker, O.G. Schmidt, K. Kern, Phys. Rev. B 72 (2005) 195320.
[17] G. Medeiros-Ribeiro, R.S. Williams, Nano Lett. 7, (2007) 223.
[18] J. Tersoff, F.K. LeGoues, Phys. Rev. Lett. 72 (1994) 3570.
[19] F.K. LeGoues, M.C. Reuter, J. Tersoff, M. Hammar, R.M. Tromp, Phys. Rev. Lett. 73 (1994) 300.
[20] T. Merdzhanova, S. Kiravittaya, A. Rastelli, M. Stoeffel, U. Denker, O.G. Schmidt, Phys. Rev. Lett. 96 (2006) 226103.
[21] A. Marzegalli, V.A. Zinovyev, F. Montalenti, A. Rastelli, M. Stoffel, T. Merdzhanova, O.G. Schmidt, L. Miglio, Phys. Rev. Lett. 99 (2007) 235505.
[22] A. Rastelli, M. Stoffel, A. Malachias, T. Merdzhanova, G. Katsaros, K. Kern, T.H. Metzger, O.G. Schmidt, Nano Lett. 8 (2008) 1404.
[23] B.J. Spencer, M. Balanariu, Phys. Rev. Lett. 95 (2005) 206101.
[24] N. Liu, J.Tersoff, O. Baklenov, A.L. Holmes, C.K. Shih, Phys. Rev. Lett. 84 (2000) 334.
[25] G. Hadjisavvas, P.C. Kelires, Phys. Rev. B (2005) 075334.
[26] C. Lang, D.J.H. Cockayne, D. Nguyen-Manh, Phys. Rev. B 72 (2005) 155328.
[27] N.V. Medhekar, V. Hegadekatte, V.B. Shenoy, Phys. Rev. Lett. 100 (2008) 106104.
[28] A. Vailionis, B.Cho, G. Glass, P. Desjardins, D.G. Cahill, J.E. Greene, Phys. Rev. Lett. 85 (2000) 3672.
[29] G. Constantini, A. Rastelli, C. Manzano, P. Acosta-Diaz, G. Katsaros, R. Songmuang, O.G. Schmidt, H. Von Kanel, K. Kern, J. Crys. Growth 278 (2005) 38.
[30] P. Kratzer, Q. Liu, P. Acosta-Diaz, C. Manzano, G. Constantini, R. Songmuang, A. Rastelli, O.G. Schmidt, K. Kern, Phys. Rev. B 73 (2006) 205347.

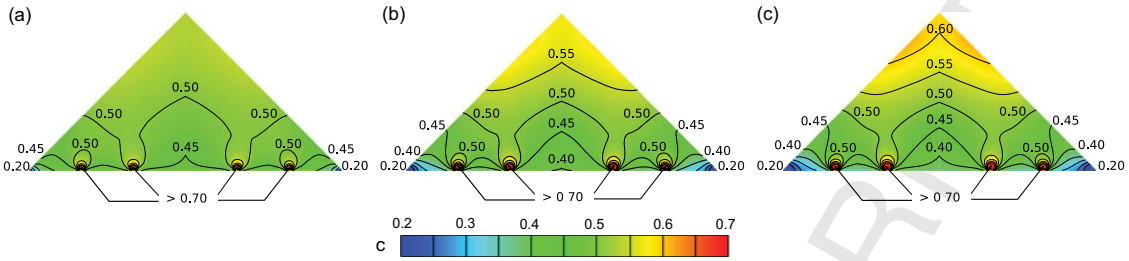

Figure 9: Influence of mixing parameter F_0 on the composition maps in dislocated nanocrystals. Equilibrium composition profiles are obtained with $F_0 = -1.06$ (a), $F_0 = -0.2$ (b), and $F_0 = -0.05$ (c). With increasing F_0 (decreasing temperature), the strain relaxation that drives the alloy segregation dominates over the thermodynamic mixing effects. The composition profiles are obtained for a misfit strain $\varepsilon_m = 0.042$, the average composition $\bar{c} = 0.5$, and the magnitude of the Burger's vector for the edge dislocation $|b| = 0.39$ nm.

[31] K. Schittkowski, Ann. Op. Res. 5 (1985) 485.
[32] Transitions in the more general case with orientation dependent surface energies and the equilibrium shapes of dots with two or more facets (Figure 5) will be considered in a forthcoming publication.
[33] J.P. Hirth, J. Loathe, Theory of dislocations, Krieger, 1992.
[34] F.K. LeGoues, J. Tersoff, M.C. Reuter, M. Hammar, R.M. Tromp, Appl. Phys. Lett. 67 (1995) 2317.
[35] J.H.G. Owen, K. Miki, D.R. Bowler, J. Mater. Sci.41 (2006) 4568.
[36] J. Sormunen, J. Riikonen, M. Mattila, J. Tiilikainen, M. Sopanen, H. Lipsanen, Nano Lett. 5 (2005) 1541.
[37] K.A. Dick, K. Deppert, L.S. Karlsson, W. Seifert, L.R. Wallenberg, L. Samuelson, Nano Lett. 6 (2006) 2842.
[38] J.L. Gray, R. Hull, J.A. Floro, App. Phys. Lett. 13 (2002) 2445.
[39] J. He, H.J. Krenner, C. Pryor, J.P. Zhang, Y. Wu, D.G. Allen, C.M. Morris, M.S. Sherwin, P.M. Petroff, Nano Lett. 7 (2007) 802.
[40] J.L. Gray, S. Atha, R. Hull, J.A. Floro, Nano Lett. 4 (2004), 2447.